Engineering Fracture Mechanics 270 (2022) 108560

Contents lists available at ScienceDirect

Engineering Fracture Mechanics

journal homepage: www.elsevier.com/locate/engfracmech

Assessing the effect of the experimental parameters in the evaluation of the essential work of fracture in high-strength thin sheets

I. Tarhouni [a,c,*], D. Frómeta [a], D. Casellas [a,b], J. Costa [c], P. Maimí [c]

[a] Eurecat, Centre Tecnològic de Catalunya, Unit of Metallic and Ceramic Materials, Plaça de la Ciència, 2, Manresa 08243, Spain
[b] Division of Mechanics of Solid Materials, Luleå University of Technology, 971 87 Luleå, Sweden
[c] AMADE, Polytechnic School, University of Girona, Campus Montilivi s/n, Girona 17071, Spain

ARTICLE INFO

Keywords:
Essential work of fracture
Fracture toughness
Advanced high strength steels
Ligament lengths range
Transition distance
Plastic zone size

ABSTRACT

The essential work of fracture methodology (EWF) has been successfully adopted to evaluate the fracture toughness of various metals and polymers. However, some aspects of the methodology are still far less understood, such as the influence of the experimental parameters on EWF measurement in thin metal sheets. In the present paper, the ligament range criterion of the EWF approach was revised for several advanced high-strength steels (AHSS). The validity of the upper and lower ligament length limits given by the ESIS protocol is redefined and rationalized according to the necking capability and the plasticity behaviour of the different AHSS grades. The work provides a new criterion to define the minimum ligament length to be tested, based on the minimum distance required by the crack to fully develop the necking capability of the material. The width constraint is too restrictive and has no effect on the deviation from linearity in the upper range. On the other hand, the maximum ligament length is proven to be controlled by the size of the plastic zone as proposed by the ESIS protocol.

1. Introduction

The growth of advanced high-strength steels (AHSS) in the automotive market is driven by the current lightweighting trend. Carmakers are turning their attention to safe and economic materials to reduce vehicle weight [1]. The outstanding combination of high strength, crashworthiness and formability shown by AHSS poses them as excellent candidates to meet the stringent lightweight and safety requirements of both present and future mobility.

Manufacturing processes for safety-related car components include different sheet metal forming, such as shear cutting, trimming, and stamping to achieve the desired formed shape. Some of these operations can reduce sheet formability and increase the risk of damage and even cracking. In this sense, the high strength of AHSS is associated with low ductility that may negatively affect sheet formability, particularly in damaged areas, as in cut or trimmed regions. Consequently, unexpected fractures may appear, compromising part quality and lowering forming process efficiency [2]. This phenomenon is known as edge-cracking, and it is found in AHSS with tensile strength higher than 800 MPa. It cannot be rationalized by conventional sheet formability approaches such as ductility values extracted from tensile tests or the forming limit diagram (FLD). Thus, the lack of a reliable criterion for characterizing edge-fracture has raised scientific and industrial interest in identifying experimental tests and material parameters that can appropriately describe and predict edge-cracking occurrence in AHSS.

* Corresponding author at: Eurecat, Centre Tecnològic de Catalunya, Unit of Metallic and Ceramic Materials, Plaça de la Ciència, 2, Manresa 08243, Spain.
E-mail address: ilef.tarhouni@eurecat.org (I. Tarhouni).

https://doi.org/10.1016/j.engfracmech.2022.108560
Received 7 February 2022; Received in revised form 22 April 2022; Accepted 17 May 2022
Available online 25 May 2022

Recently, fracture toughness, measured in the frame of fracture mechanics, has been proposed as a material property for characterizing edge fracture resistance in metallic sheets [3–7]. It has been experimentally proved for many AHSS grades that toughness readily describes edge cracking resistance, i.e., steels with low fracture toughness are more sensitive to edge cracking than tougher steels. Furthermore, a good correlation has been obtained between fracture toughness and impact resistance for several AHSS steel grades [8]. Therefore, automotive engineers and designers are increasingly interested in fracture toughness as a key material parameter for the design of safer and lighter structural components.

One of the first challenges in the characterization of fracture toughness in ductile thin sheets is the development of a large plastic zone prior to crack initiation. The standardized testing methods [9] for linear elastic fracture mechanics (LEFM) limit the plastic zone size to a small area in front of the crack tip. Hence, it cannot be adopted for fracture toughness assessment of ductile sheet metals such as AHSS. Elastic plastic fracture mechanics (EPFM) overcomes this limitation and should be used to characterize the fracture resistance of AHSS. In the frame of EPFM, *J-integral* and crack-tip opening displacement (CTOD) are well-accepted methods. The experimental procedures for the determination of *J-integral* are standardized in ASTM-E1820 [10]. The advantage of this method is its ability to account for greater plasticity near the crack tip and the specimen's size restrictions are less stringent compared to LEFM. However, the sheet thickness of AHSS used in the automotive industry (usually in the range of 1 to 3 mm) does not meet the requirements stated in ASTM-E1820, so its direct application to characterize the fracture toughness of thin sheets is doubtful. Frómeta et al. [11] investigated the relevancy of *J-integral* alongside other methodologies for the fracture toughness evaluation of thin AHSS sheets. The work showed that *J-integral* cannot properly characterize the overall crack propagation resistance of steels showing a significant energetic contribution from necking during crack propagation, as occur in most of the AHSS grades, where the values of *J-integral* underestimate the total fracture resistance. In addition, the complex and elaborate test set-up and data handling make the tests difficult to perform. Alternatively, the essential work of fracture (EWF) methodology, which accounts for the energetic contribution of crack initiation and propagation, can provide more information about the overall fracture process. This work concludes that the EWF methodology is the most recommendable to measure crack propagation resistance, i.e., the fracture toughness, of thin sheets. Some other works have shown that this approach is perfectly suited for thin metal sheets and especially for AHSS [4–8,12–15].

The EWF approach [16] was developed to evaluate ductile fracture toughness under plane stress dominant conditions. The method is applicable to any specimen geometry. However, double-edge-notch-tension (DENT) specimens are the most used. The area between the two symmetric notches in DENT specimens, known as ligament (l), is subjected to a tensile stress, without risk of buckling, which implies that cracks always grow under mode I [17]. The EWF method is based on the energy partitioning of geometrically similar DENT specimens with different ligament lengths. Given that the ligament is fully yielded, and the plastic zone is confined within the ligament zone, a linear regression of the total work dissipated during the fracture process against the ligament length gives the energy spent in the creation of a surface in front of a propagating crack, i.e., the fracture toughness. Therefore, this approach has been gaining acceptance recently, due to its relative experimental simplicity. The concept is currently well-established and accepted in assessment of the fracture toughness of ductile metal sheets [12–15,17,18], AHSS [4,5,11,19–22], high strength aluminum alloys [23] and polymers [24]. However, the method is not standardized for metallic sheets, and the existing testing protocol from the ESIS TC4 [25] provides guidelines for its effective application in plastics and composites, without any recommendations for metal sheets. Additionally, some works have questioned the validity of the experimental constraints of this protocol, stating that some of them are material-dependent and that these parameters cannot be extended to other testing conditions [26–28]. Therefore, numerous research works on testing methodology, valid ligament range, linear fit, etc. are still ongoing [26–30].

Two of the most important parameters influencing the accuracy of EWF measurements are the notch root radius and the ligament range. This is well-reported for polymers [31] but less information is available for metals. Although LEFM and EPFM clearly state that fatigue pre-cracks should be used to evaluate fracture toughness, few works have addressed this topic for EWF. The recent work of Frómeta et al. [11] examined the effect of notch root radius on fracture toughness in AHSS, using notched and fatigue pre-cracked specimens. The work stated that the EWF is highly influenced by notch radius and may provide misleading results in materials with a very high notch sensitivity. Thus, fracture toughness in high strength materials, such as AHSS, can be only accurately measured using specimens containing very sharp notches, typically fatigue-induced pre-cracks or sharp notches induced with specific notching devices [11,32].

The main source of experimental deviations in the measurement of EWF is the use of an incorrect ligament range. Cotterell and Reddel [16] indicated that the minimum ligament length should be 3–5 times the specimen thickness (B). This lower limit is assumed to be related to the plane strain/plane stress transition [33]. Consequently, a very small ligament could lead to an increase in stress triaxiality and a transition to the mixed stress state (plane stress–plane strain). The upper limit is taken as the minimum value between the plastic zone size (r_p) and the ratio of the total width of the specimen (W)/3. It intends to avoid the contained yielding of the ligament zone and the asymptotic transition to plane stress fracture toughness (Gc) determined from LEFM [17,27].

Some authors have addressed the validity of ligament range in the evaluation of EWF in polymers. Wu et al. [33] found for commercial polybutylene terephthalate/polycarbonate/impact modifier (PBT/PC/IM) blend that the slope of the linear fit increased at larger ligaments. According to the authors, this deviation is not related to the ratio $W/3$ or the plastic zone size (r_p) but to an important increase in the plastic zone size at the critical crack length/width ratio (a/W). Similarly, Hashemi et al. and Arkhireyeva et al. [34–36] observed that the linearity of some thin polymer sheets could be achieved even above the limit ($W/3$). They stated that this constraint was too restrictive for polymers. Tuba et al. [27] argued that the localized necking in ductile polymers stabilizes the plastic zone and maintains the uncontained yielding. On the other hand, for metals, when extensive plasticity occurs and necking is not significant, the plastic zone size could influence the uncontained yielding. The lower ligament limit has also been studied by

Table 1
Chemical composition in [mass%] of the investigated steels. The balance is Fe.

Material	C	Si	Mn	Cr	B	Al	Ti
CP1000	~0.1	<0.5	1.8–2.2	<0.7	<0.003	–	–
DP1000-A	~0.15	<0.5	~0.23	<0.7	<0.003	~0.05	<0.0060
CFB1180	~0.23	<2.0	<2.9	<0.7	<0.005	~0.04	~0.0070
DP1000-B	0.08	0.26	~0.26	0.31	0.0018	0.16	0.0372

Table 2
Tensile properties of the tested steels: yield strength (σ_{YS}); ultimate tensile strength (σ_{UTS}) ; uniform elongation (UE); total elongation (TE).

Material	σ_{YS} (MPa)	σ_{UTS} (MPa)	UE (%)	TE (%)
CP1000	915	1008	4.80	8.8
DP1000-A	807	1057	6.54	9.7
CFB1180	987	1219	9.20	12.6
DP1000-B	733	1040	5.35	8.7

Tuba et al. [27]. The authors stated that the increase in net-section stress in small ligaments in some metals, like copper and polymers is not necessarily related to plane strain/plane stress transition, but to a non-ideal behaviour of the material such as initiation under 3D state and plasticity prior to crack initiation. Thus, the lower bound in this case is overconservative. Marchal et al. [29] also found that the minimal limit could increase to (6–8)B for polymers based on a statistical analysis.

Most of the studies mentioned above addressing the validity of ligament range are focused on polymeric materials. As a result, the definition of some of the experimental parameters for metallic materials is still an open question and needs to be further explored. The possibility of testing specimens with sizes outside of the current ESIS protocol and, thus, decreasing experimental constraints is appealing in terms of boosting the fracture toughness evaluation of metal sheets. For instance, if small ligaments can be used, small specimens can be extracted from formed parts. Or less material will be required, which will facilitate material characterization at the development stage. Accordingly, the aim of this work is to better define the experimental parameters of the EWF test and to provide practical guidelines for its appropriate use in thin metallic sheets. Attention is focused on set ligament range limits, since the effect at the notch root radius has been well-defined in previous works [11]. The upper and lower limits of ligament length as defined in the ESIS protocol will be assessed and redefined to meet the particularities of the AHSS. In this regard, four AHSS grades with markedly different mechanical and fracture behaviour are tested. Results will be rationalized in terms of hardening capacity, necking capability, size of the plastic zone and overall mechanical properties.

2. Materials and methods

The experimental tests were carried out on four grades of cold-rolled AHSS sheets with different microstructure and mechanical properties: complex-phase (CP1000), carbide-free bainitic (CFB1180) and two dual-phase (DP1000) named in this paper as DP1000-A and DP1000-B. Scanning electron microscopy (SEM) analysis was performed to obtain the microstructure (Fig. 1). The microstructure of CP1000 reveals homogeneous bainite/tempered martensite matrix (Fig. 1(a)). DP1000-B presents ferritic-bianitic matrix with martensite islands homogeneously distributed (Fig. 1(b)). CFB1180 microstructure consists of ferrite and bainite matrix with significant amount of metastable retained austenite (Fig. 1(c)). DP1000-A presents ferrite (α) bainite/tempered martensite (α) matrix with some dispersed martensite and fresh martensite/retained austenite (M/RA) islands, there is also the presence of carbide precipitates within B/TM grains (Fig. 1(d)). The chemical composition of each material is listed in Table 1. The tensile properties, summarized in Table 2, were obtained by conventional tensile tests according to ISO 6892-1 [37]. Tests were conducted on specimens oriented transversally to the rolling direction. True stress–strain curves (Fig. 2) and the strain hardening were used to understand the deformation behaviour of the studied steels. Some research works [38,39] have shown that the strain hardening behaviour of AHSS is not constant and could considerably change with plastic deformation, which means that it is hard to describe the strain hardening using only one value. Accordingly, the hardening capacity of the studied steels was analysed using the instantaneous strain hardening exponent, $n_i(\epsilon)$ (Fig. 3), given by the following equation:

$$n_i(\epsilon) = \frac{\mathrm{d}\ln\sigma}{\mathrm{d}\ln\epsilon} \tag{1}$$

Where σ is the true stress and ϵ is the true strain.

The EWF methodology assumes that the total work of fracture in the crack tip region can be split into two parts: the work consumed in the fracture process zone (FPZ), named as the essential work of fracture (w_e), and the plastic work generated in the outer region surrounding the FPZ, named as the non-essential work of fracture (w_p):

$$W_f = W_e + W_p = w_e Bl + w_p \beta B l^2 \tag{2}$$

Where B is the sheet thickness, l is the ligament length, and β is a non-dimensional shape factor (geometry dependent).

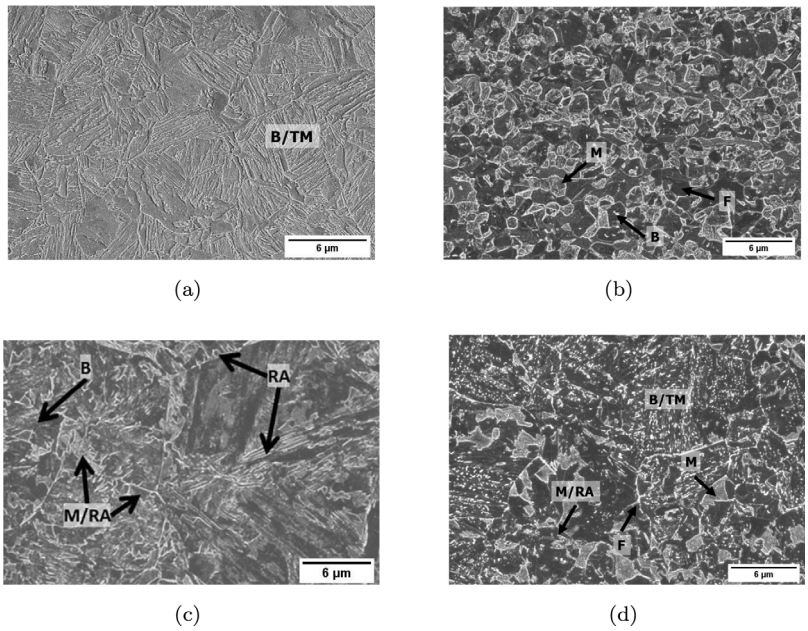

Fig. 1. SEM micrographs of the tested steels. (a) CP1000; (b) DP1000-B; (c) CFB1180; (d) DP1000-A. B: Bainite, TM: Tempered Martensite, M: Martensite, F: Ferrite, RA: Retained Austenite.

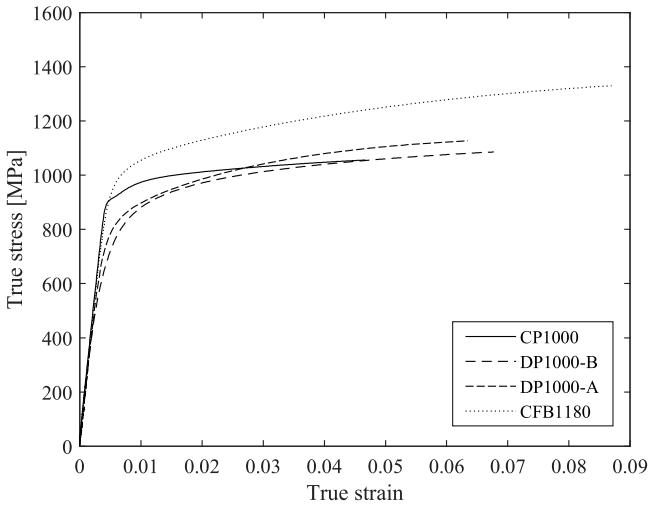

Fig. 2. True stress–strain curves of the tested steels.

w_e is proportional to the fracture area and w_p is proportional to the volume of the plastic zone. Accordingly, the two works of fracture can be separated by testing geometrically similar specimens with different ligament lengths. Applying a linear regression to data set of the specific work of fracture against l, allows to obtain w_e and w_e values [16]. Since Eq. (2) is valid only under plane stress condition, the ESIS protocol [25] proposes a lower limit (l_{min}) proportional to the thickness. It is suggested that the limit l_{min} should be larger than 3 or 5 times the sheet thickness, or alternatively be of 5 mm. The ESIS protocol also defines an upper limit for the ligament length (l_{max}) determined by the minimum values of two parameters; the size of the plastic zone (r_p) and one third of the specimen width (W), i.e.$W/3$. An arbitrary l_{max} value of 15 mm is also proposed by the protocol for practical reasons. According to Irwin, the size of the plastic zone is estimated based on linear elastic crack-tip stress fields and it is calculated according to Eq. (3) using the Young's modulus (E), and the yield strength (σ_{YS}) [29]:

$$r_p = \frac{1}{\pi}\frac{Ew_e}{\sigma_{YS}^2} \tag{3}$$

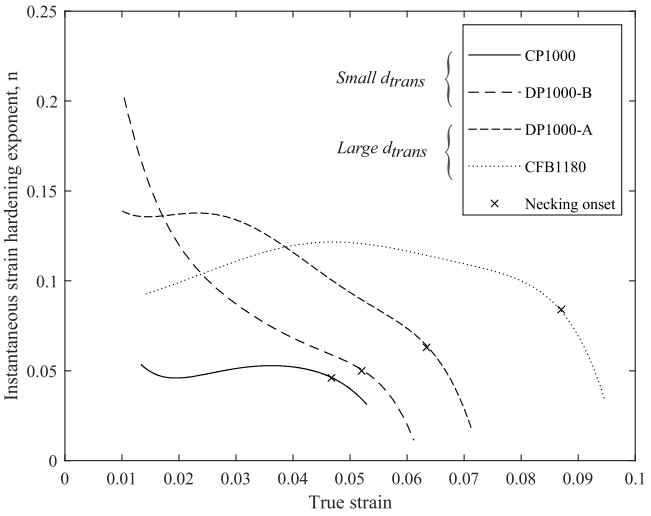

Fig. 3. Instantaneous strain hardening exponent as a function of true strain. The cross (x) indicates the onset of necking, corresponding to the uniform elongation in engineering stress–strain curves obtained in conventional tensile tests.

Table 3
The ligament length used according to the range.

	Small ligament range	Conventional ligament range (following ESIS protocol)	Large ligament range
Ligament length l [mm]	$2 < l < 5$	$6 < l < 15$	$l > 15$

The EWF tests were conducted on DENT geometry using 13 specimens of different initial crack lengths between l_{min} and l_{max}, according to the ESIS protocol guidelines [25]. Considering that there is not a clear definition of l_{min} and the protocol stated that this constraint varies from one material to another, an l_{min} of 6 mm was chosen as the lower limit for all of the tested steels herein. This 6 mm corresponds to 4 times the specimen thickness, which lies within the range 3–5 times B stated by the ESIS protocol. An l_{max} value of 15 mm was selected as an upper limit to avoid a possible contained yielding. The validity of this limit was experimentally checked after the tests using the Digital Image Correlation (DIC) technique. Accordingly, the ligament lengths used for the calculation of the EWF were between 6 and 15 mm. The ligaments within this range will be here referred to as *conventional* ligaments.

Another series of specimens with ligament lengths lower than l_{min} and larger than l_{max} were tested. They will be here referred to as *small* ligaments and *large* ligaments respectively, to differentiate from the *conventional* ligament range. The experimental tests on the *conventional* ligament range showed that a ligament length of 6 mm fits well with the linear trend. Due to the experimental difficulty in achieving ligaments below 2 mm, the *small* ligaments range between 2 mm to 5 mm. Ligament lengths above 15 mm were used for the *large* ligament range. Considering the loading capacity of the testing machine, the maximum length tested for this range of ligaments is 40 mm. The ligament lengths used for each range are summarized in Table 3. Between 6 to 8 specimens were tested in each range.

The size of the DENT specimens was 200 mm height, 55 mm width, and the sheet thickness was of 1.5 mm for the four studied AHSS. The notches were machined by electrical discharge machining, resulting in a notch tip radius of 150 μm. A fatigue pre-crack of about 1 mm of length was induced on each side, following the conditions given in [37]. The ligament length, i.e., the distance between the two fatigue pre-cracks from both edges, was accurately measured after the fracture of the specimens by optical microscopy. The tests were performed at room temperature and quasi-static loading of 1 mm/min until complete fracture occurred. The load-line displacement curves were measured by a video extensometer, using an initial gauge length of 50 mm. The total work of fracture (w_f) generated during the test was obtained by integrating the area under the load–displacement curves and normalizing it by the net area. Optical microscopy was used after the fracture test to examine the fracture surface of specimens with *small* ligament lengths. DIC technique was employed to examine the surface strain field in *large* ligaments and check the full yielding condition prior to crack initiation.

3. Results

As already stated in the introduction, stress triaxiality tends to increase below a certain ligament length and a transition to the mixed-mode regime is expected to take place. Under this condition, Eq. (2) cannot be applied and the linearity of w_f vs l data is lost. This transition is assumed to occur when ligament length is relatively short compared to specimen thickness [40]. To experimentally check the validity of Eq. (2) for *small*, *conventional*, and *large* ligament lengths, the values of the specific total work of fracture, w_f, for all these ligament ranges were plotted against l for the 4 studied steels (Fig. 4). The full ligament yielding condition at l_{max}

Table 4
EWF results obtained from the least squares regression fits of the *conventional*, *small*, and *large* ligament ranges. R is the correlation coefficient of the linear regression.

Steel grade	*Conventional* ligament range			*Conventional* + *Small* ligament range			*Conventional* + *Large* ligament range		
	w_e [kJ/m^2]	w_p [MJ/m^3]	R^2	w_e [kJ/m^2]	w_p [MJ/m^3]	R^2	w_e [kJ/m^2]	w_p [MJ/m^3]	R^2
CP1000	405 ± 11	12 ± 1	0.93	291 ± 19	22 ± 2	0.82	415 ± 7	12 ± 0	0.98
DP1000-A	149 ± 21	24 ± 2	0.93	141 ± 12	24 ± 1	0.94	188 ± 11	20 ± 1	0.98
CBF1180	104 ± 30	34 ± 5	0.92	116 ± 14	33 ± 2	0.96	177 ± 16	27 ± 1	0.98
DP1000-B	286 ± 17	23 ± 1	0.96	189 ± 15	31 ± 2	0.96	339 ± 14	18 ± 1	0.97

was checked after the test using DIC, as mentioned above. For all the steels tested, all the ligaments up to 15 mm were completely yielded. As a result, a good linear fitting was obtained for the conventional ligament range. These ligaments were used to calculate the right value of essential work of fracture, w_e (Table 4).

For the *small* ligament range, two different behaviours can be discerned (Fig. 4). For DP1000-A and CFB1180, the values of w_f obtained with *small* ligaments follow the linear regression obtained by *conventional* ligaments. Hence, no transition from plane-stress to the mixed mode stress state is observed. Indeed, including *small* ligament specimens in the calculation of w_e increased the correlation coefficient R^2 and does not significatively alter the final value of w_e of 141 ± 12 kJ/m^2 for DP1000-A and 116 ± 14 kJ/m^2 for CFB1180 (Table 4). On the other hand, for CP1000 and DP1000-B a clear deviation from the linear fit of the *conventional* ligament range is observed, indicating a deviation from the plane stress state at l approximately equal to l_{min} (6 mm). The w_e values obtained from the valid ligaments are w_e of 405 ± 11 kJ/m^2 for CP1000 and w_e of 286±17 kJ/m^2 for DP1000B. However, the extrapolation of the short ligaments results in a lower value than the valid w_e. The deviation from the linear fit is more significant in the case of CP1000 compared to DP1000-B, thus, decreasing R^2 from 0.93 to 0.82. These results indicate that the plane-stress/plane-strain transition depends on the material to be tested.

The behaviour of *large* ligaments is different for each material. In the case of CP1000 *large* ligaments follow the linear trend shown by *conventional* ligaments, with very good linear fitting. The use of *large* ligaments increases the accuracy of w_e, by reducing the standard deviation and R^2. For DP1000-B, *large* ligaments follow the regression line up to a l value of 26.2 mm; as the ligament gets larger, a progressive deviation is observed, resulting in an increase of w_e of 339±14 kJ/m^2. For DP1000-A and CFB1180 the *large* ligaments totally deviate from the linear trend of the *conventional* ligaments. The slope of curves decreases as the ratio l/B increases, resulting in lower βw_p values. The width restriction ($W/3$) has no noticeable effect on the EWF results as the linearity is achieved for the ligaments above this limit, 18 mm. As a result, this constraint for upper ligament length can be disregarded for AHSS if the minimum value corresponds to $W/3$.

4. Discussion

4.1. Fracture surface analysis

The total work of fracture obtained with *small* ligaments differs from the valid ligament range for two materials (CP1000 and DP1000-B). Whereas in CFB1180 and DP1000-A both the *small* and the *conventional* ligament lengths have the same trend. The distance between the two crack fronts in DENT specimen, i.e., the ligament length, affects the stress–strain state, so a detailed analysis of the fracture surfaces was performed to understand the different behaviour among the studied steels (see Fig. 5). All the tested specimens exhibited a typical ductile fracture, as expected. The fracture surface shows three different regions: (i) a flat mode I fracture surface corresponding to the propagation of the fatigue pre-crack; (ii) a triangular shape surface in the centre of the specimen just ahead of the flat fatigue pre-cracked surface, associated with crack initiation under 3D stress state; and (iii) a gross fracture profile of the stable crack growth varying between completely slant and flat shifted to slant fracture depending on the steel. This is the common fracture morphology of the DENT specimens, discussed in detail in Ref. [39].

The first difference in the surface characteristics for the studied steels is that DP1000-A and CFB1180 experience less thickness reduction (Figs. 5(e) and (g)), compared to CP1000 and DP1000-B, where the specimen thinning is evident after a certain crack propagation (Figs. 5(a) and (c)). The amount of necking developed in CP1000 and DP1000-B reaches a uniform level after a significant crack growth. The zone between the crack initiation and the necking stabilization is marked by a mode I flat surface with a tunnelling triangular shape as shown in Figs. 5(a–d) and 6(a). Some authors have referred to this effect in previous publications as a “transition distance” [18,41]. The tunnelling zone is characterized by a dominant plane-strain stress state and a flat fracture surface that becomes a typical thin metal sheets slant fracture. This transition distance is reduced to the small triangular shape in the case of DP1000-A and CFB1180. Figs. 5(e–h) and 6(b) show that after the crack initiation and the formation of the triangular zone, a uniform slant fracture is readily developed. It is well known that the dominant stress state in thin plates is plane stress. However, at high loading conditions, the constraints applied to the crack tip by the surrounding materials to prevent it from propagating in the x-axis defined by the crack propagation direction and the z-axis defined by the thickness direction, create a triaxial state of stress. Accordingly, the plane stress state exists only at the edges of the specimen and far from the crack tip. At mid-thickness and in front of the crack tip, at a distance small compared to the thickness of the specimen, the triaxiality is high and the material is under plane strain [42,43]. Knockaert et al. [44] evaluated the stress distribution numerically at fracture initiation in thin DENT steel plates. The numerical model showed high stress triaxiality at mid-thickness and little farther from the crack tip. The value exceeds

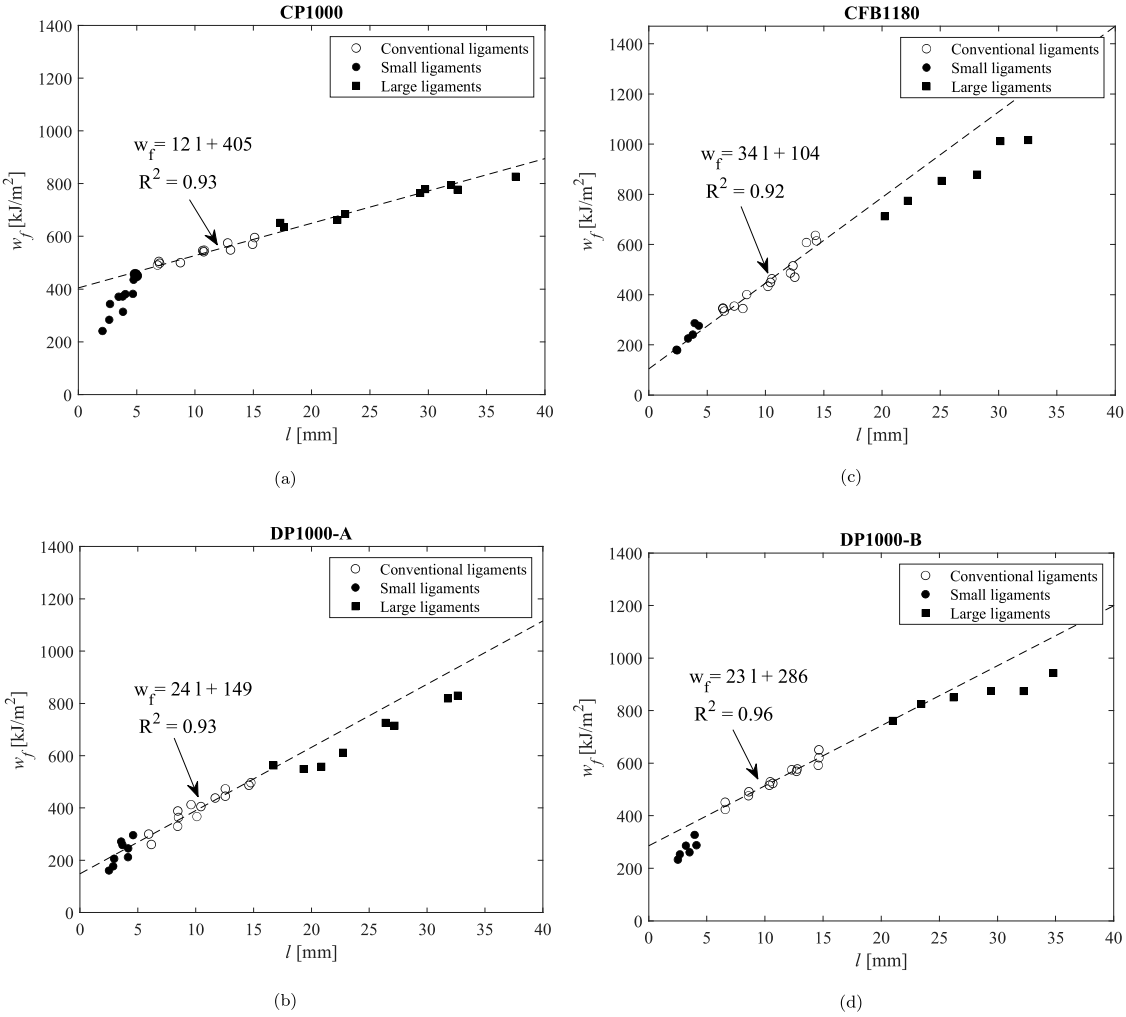

Fig. 4. The total specific work of fracture w_f for the tested steels as a function of the ligament l for the *conventional*, *small*, and *large* ranges. The dashed line is the linear fit through the *conventional* ligament lengths range. (a) CP1000; (b) DP1000-A; (c) CFB1180; (d) DP1000-B.

1/3 of uniaxial tension to reach 0.99 as reported by the authors. Accordingly, After the initiation, the crack tends to propagate in the region of high triaxiality, resulting in this triangular tunnel shape and flat surface in both categories of materials.

To better understand the failure mechanism and the difference in the macroscopic appearance of the fracture surface in these materials, the fracture surface characteristics at the microscopic level were assessed by SEM. The inspections were directed at different locations on the fracture surface: the triangular flat surface, the flat transition zone in the case of CP1000 and DP1000-B, and the slant zone for DP1000-A and CFB1180. Typical ductile fracture morphology featuring dimples was observed in the four materials (Fig. 7), with two different types of dimple populations: large dimples and fine dimples. The triangular flat surface contains exclusively large dimples, indicating that the crack initiates at high stress triaxiality. The transition distance in CP1000 and DP1000-B, reveals a rough surface dominated also by large dimples (Figs. 7(a) and (b)), whereas, DP1000-A and CFB1180 slanted zone presents a smoother surface, mostly formed by fine dimples with only a limited number of large dimples (Fig. 7(c) and (d)).

4.2. Relationship between strain hardening and d_{trans}

From the experimental observation, the large transitional distance occurs in materials with high necking capacity but absent in materials with low necking capacity (Fig. 5) . To elucidate the mechanism behind the development of the transition distance and investigate any possible relationship with the necking capacity, the failure mechanisms of ductile metal sheets should be disclosed. The fracture of ductile metals involving voids nucleation, growth and coalescence arises from the interaction of two factors: porosity characterized by void population, and plastic flow localization characterized by materials hardening [45]. Two macroscopic modes of failure resulting from plastic localization can be distinguished in tensile tests: (a) failure by plastic instability "void sheet" without severe necking and (b) failure by void coalescence with extensive necking [46–48].

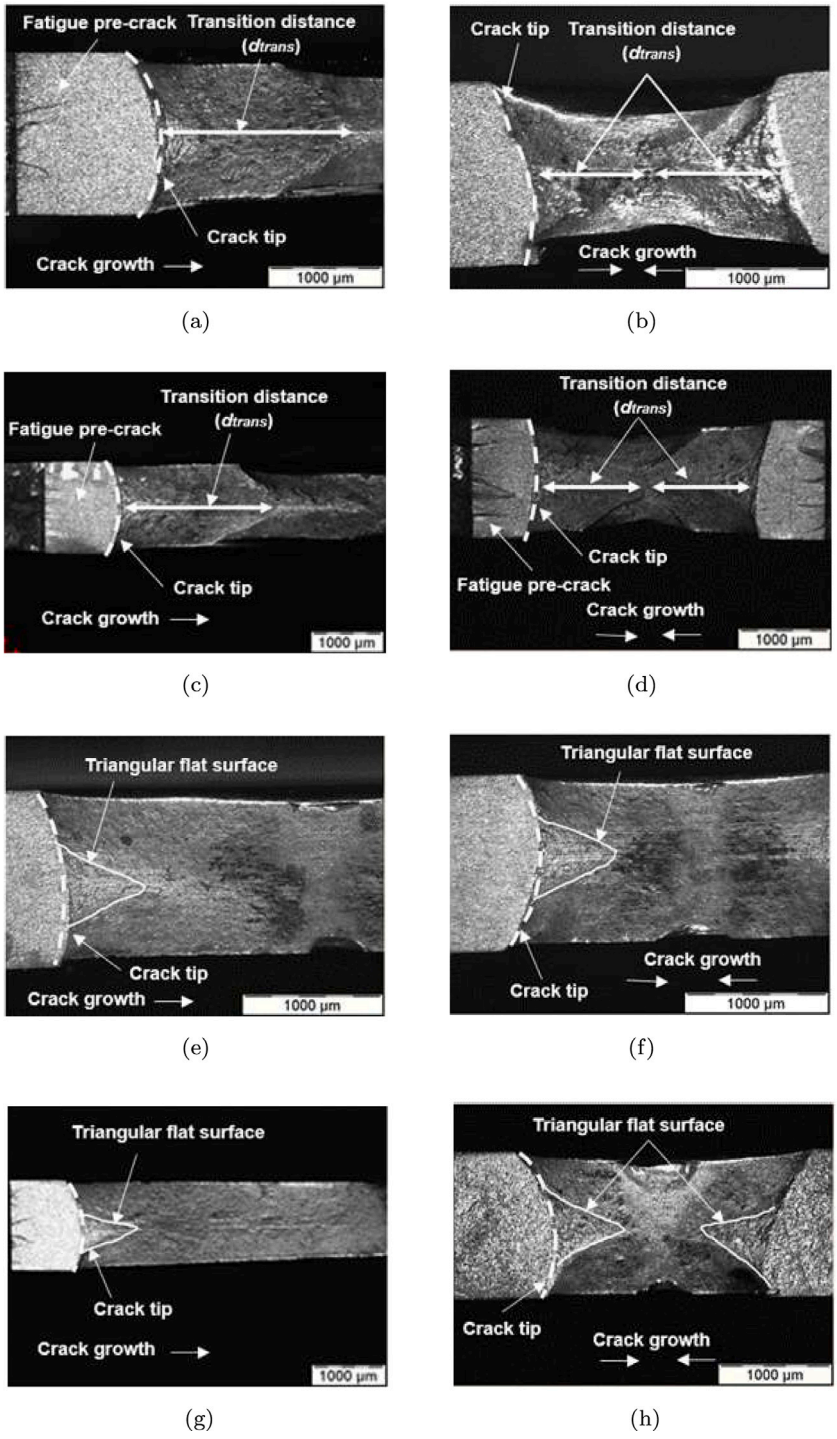

Fig. 5. Optical microscopy images of the fracture surface. (a, b) CP1000; (c, d) DP1000-B; (e, f) DP1000-A; (g, h) CFB1180. (a, c, e, g) correspond to specimens of the *conventional* ligaments range. (a) l = 14.9 mm, (c) l = 14.5 mm, (e) l = 10.4 mm and (g) l = 10.5 mm; (b, d, f, h) correspond to specimens of the *small* ligaments range. (b) l = 2.0 mm, (d) l = 2.7 mm, (f) l = 2.5 mm and (h) l =2.4 mm.

At a microscopic level, the high stress triaxiality in metallic thin sheets promotes nucleation and growth of voids (primary) in the necking zone. These voids, formed at an early stage of the deformation, can grow and become large voids [48]. Materials with low hardening capacity exhibit necking at low strains. Accordingly, the matrix surrounding the voids deforms, allowing the primary voids to grow into large dimples. These dimples subsequently coalesce and connect to each other resulting in a fracture.

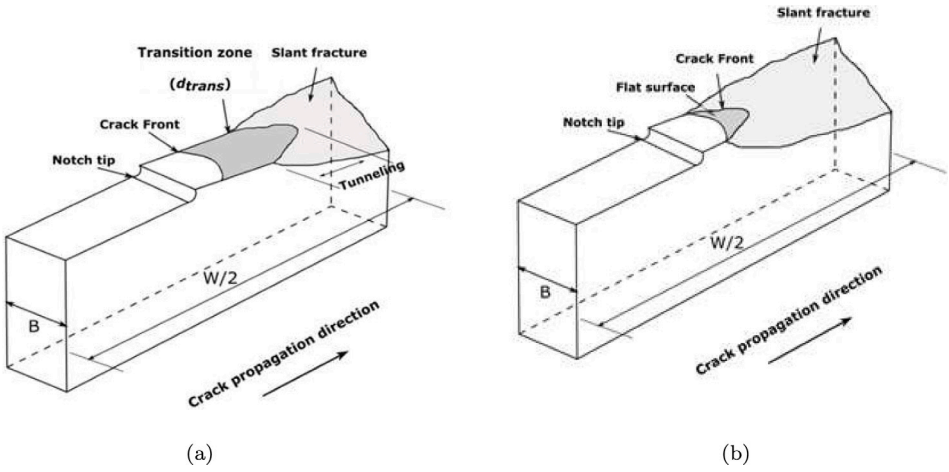

Fig. 6. A schematic representation of the different ductile fracture surfaces of the investigated steels. (a) A transition from flat to slant fracture spotted in CP1000 and DP1000-B. The transition region can be seen connecting the flat fatigue pre-crack and the slant growth; (b) A slant fracture such is the case of CFB1180 and DP1000-A.

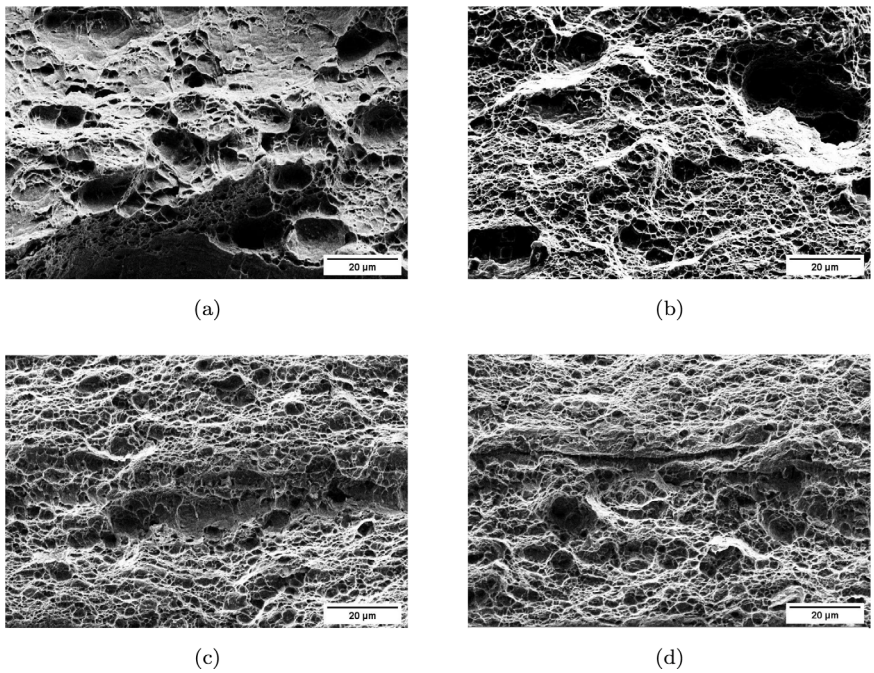

Fig. 7. Microscopic fracture surface morphology of the *conventional* ligament range by SEM at: (a) CP1000 in the transition zone; (b) DP1000-B in the transition zone; (c) DP1000-A in the slant zone; (d) CFB1180 in the slant zone.

The fracture surface in this mode consists of a flat surface with large dimples as observed in CP1000 and DP1000-B (Figs. 7(a) and (b)). In materials with high strain hardening capacity, the onset of necking is delayed, consequently, the nucleation of the primary dimples is also retarded. This allows the nucleation of smaller voids (secondary) at higher strain value. During necking, voids can nucleate and grow, simultaneously, the matrix hardens due to plastic strain, hindering the growth of these voids. The increase in the stress leads to plastic instability and plastic localization along the maximum shear stress. The primary voids connect to each other and form a crack through the secondary voids leading to fracture and failure by "void sheet" [48]. This mechanism features two populations of dimples: large dimples that formed during the necking and small dimples that nucleate during the failure. This type of fracture is observed in the SEM images of DP1000-A and CFB1180 (Fig. 7(c) and (d)) [47–49].

As it is commonly acknowledged that the strain hardening capacity plays an important role in material's necking [15,19,46] and in the promotion of the mode of fracture [47,48], the strain hardening behaviour of the studied steels was analysed using Eq. (1). Fig. 3 shows the instantaneous strain hardening exponent, n_i, as a function of the true strain. The onset of diffuse necking in the

tensile test is also added in Fig. 3. It is noteworthy that the variation of n_i with the plastic strain is remarkably different from one steel to another. For CP1000 and CFB1180, the instantaneous n_i is nearly constant and slightly decreases after the onset of diffuse necking. However, n_i constantly decreases as strain increases in the case of DP1000-A and DP1000-B. For DP1000-A, n_i maintains a constant value at low deformation then continuously decreases with the increase of the plastic strain. DP1000-B exhibits a sharp drop in n_i from the initial stages of deformation. In order to rationalize the crack propagation behaviour, the attention is directed to the values of n_i after the initiation of necking (marked by a cross, x, in Fig. 3). It can be discerned that CFB1180 and DP1000-A uphold a higher strain hardening exponent than CP1000 and DP1000-B around this point. Experimentally, it can be deduced that materials with low n_i i.e., CP1000 and DP1000-B exhibit more pronounced and localized necking with significant thickness reduction, while materials with high n_i i.e., CFB1180 and DP1000-A demonstrate smaller and smoother necking zone. Hence, the increase of the strain hardening exponent leads to less necking and small dtrans. On the other hand, a low strain hardening exponent results in higher necking and permits development of a large d_{trans}. Such results indicate that the hardening exponent and the necking capacity of the materials can give an insight into the fracture mode and the size of d_{trans}.

4.3. Influence of ligament length on d_{trans}

Fig. 8 presents the transition distance (d_{trans}) as a function of the ligament l for the four steels. For CP1000 and DP1000-B, d_{trans} corresponds to the whole flat surface, whereas for DP1000-A and CFB1180, the d_{trans} is associated with the length of the triangular shape. It is evident that the transition distance depends on the material tested and is mostly independent of the ligament length.

As the ligament gets shorter, i.e., small ligaments, the fracture morphology changes for some steels. The fracture surface of the small ligament specimens in CP1000 and DP1000-B (Fig. 5(b) and (d)) shows that when the whole ligament is consumed by the transition distance ($l \approx d_{trans}$), there is no necking stabilization area. Cotterell et al. [17] stated that the ligament length should be larger than this transition distance, labelled in his work l_{trans}, so that the fracture initiated under plane strain state can change to plane stress when l is larger than l_{trans}. In *small* ligaments, the difference between l and d_{trans} decreases and thus the ability of the material to develop its full necking capacity may be compromised. Theoretically, there should be a minimum distance the crack should grow to guarantee the transition from plane strain state to plane stress state. The DENT specimen has two crack fronts, one at each side, so they grow towards the middle of the specimen. Thus, the minimum ligament length to assure a complete necking development for each crack is 2 d_{trans}. However, considering experimental scatter and the difficulty in accurately measuring this distance in some materials, this minimum ligament length should be at least equal to a minimum length of 3 d_{trans} (2 d_{trans} ± the uncertainty). Consequently, when ligament length is equal or lower than 3 d_{trans}, it remains in a quasi-plane strain state, leading to a deviation in the value of the work of fracture for short ligament length specimens. This is the case for CP1000 and DP1000-B with d_{trans} of 1.11±0.47 mm and 2.19±0.38 mm respectively, where ligaments lower than 3 mm and 5 mm deviate from the trend of *conventional* ligaments (Figs. 4(a) and (d)).

In the case of DP1000-A and CFB1180, the high hardening capacity of the materials results in a very low degree of necking and a very short transition distance (triangular flat surface) equal to 0.72±0.05 mm for CFB1180 and 0.58±0.04 mm for DP1000-A, as mentioned above. The ligament in this case shifts to plane stress regime in a relatively short distance. Therefore, the 3 d_{trans} condition is always fulfilled with these materials, given that it is experimentally difficult to test ligament lengths lower than 2 mm. This explains the similar behaviour between *small* and *conventional* ligaments for these steels (Figs. 4(b) and (c)). Accordingly, the results would confirm that pure plane stress state does not exist, and the stress state is related to the ratio l/d_{trans}. In general terms, it can be stated that the lower ligament limit is for ligament lengths that satisfy the condition $l/d_{trans}>3$. The lower limit imposed by the protocol [25] seems to be practical for high necking ability materials if d_{trans} is unknown. However, this restriction is too conservative for low necking capability materials.

4.4. Influence of plastic zone size on large ligaments

Regarding *large* ligaments, Fig. 4 shows that some ligaments deviate from the regression line of the *conventional* ligaments. It is conventionally accepted that the upper ligament bound is linked to the full ligament yielding criterion. Accordingly, the strain field prior to crack initiation was analysed by means of ARAMIS DIC software in *conventional* and *large* ligaments. The presence of the plastic deformation was evaluated by means of the equivalent Von Mises strain. Its value is derived from the deviatoric strain tensor in a similar way to the equivalent Mises stress, assuming plastic incompressibility and plane stress state [50]. The strain magnitude represents the deformation state at each point of the analysed surface. The material is considered yielded if the total strain exceeds a threshold value of 0.5%, corresponding to the yield stress. The analysis was carried out up to the onset of the crack detected by a video camera, since crack initiation in thin metal sheets generally takes place just before P_{max}. Fig. 9 shows the Von Mises strain at the crack initiation for the four tested steels in some *conventional* and *large* ligaments, the scaling factor is set between 0 and 1% of deformation. At first sight, a transition from a more circular-elliptical shape in *conventional* ligament lengths (Fig. 9(a–b)) to a diamond-like shape in *large* ligaments (Fig. 9(c–f)) can be seen. From such observations of the plastic zone size of the deviated ligament lengths, it is readily apparent that the full ligament yielding criteria is not fulfilled in these specimens. This confirms that the deviation from the linear fit at a certain ligament length for the investigated steels is related to the contained yielding at crack initiation.

To further validate the above statement, the plastic zone size (r_p) was estimated according to Irwin's plastic zone size through Equation (2). The calculation of r_p aims to provide information about the maximum ligament length that satisfies the uncontained yielding condition. Results are presented in Table 5. It is evident from Fig. 4 and Table 5 that the beginning of the offset from the

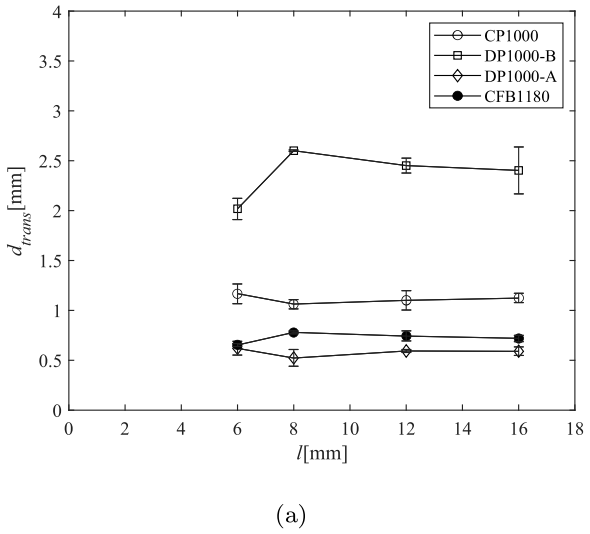

(a)

Fig. 8. Transition distance (d_{trans}) as a function of the ligament length (l) for *conventional* ligaments. The mean value is provided in the plot.

Table 5
The plastic zone size (r_p) estimation using Eq. (3).

Material	r_p [mm]
CP1000	32
DP1000-A	16
CFB1180	14
DP1000-B	30

linear fitting given by *conventional* ligaments corresponds exactly to a ligament length value larger than r_p. For instance, a deviation from the linearity is observed at l equal to 37.5 mm in CP1000 and l equal to 29.4 mm for DP1000-B. In the cases of CFB1180 and DP1000-A, almost the whole ligament range is offset from the regression line because of the small size of the plastic zone (14 and 16 mm). Therefore, it can be fairly stated that the upper ligament limit defined by the protocol is still valid in the case of AHSS.

5. Conclusions

Based on the experimental values of the work of fracture obtained with a wide range of ligament lengths of four different AHSS grades, and according to the experimental observations on the crack propagation area, the fracture surfaces, and on the DIC analysis, the following conclusions can be drawn:

- The minimum ligament limit l_{min} proposed by the ESIS protocol appears to be too conservative for some AHSS. The results showed that the linearity between w_e and l can still be achieved, even below l_{min} for some steels. This depends on the hardening and necking capability of the tested material.
- Steels with high necking ability (CP1000 and DP1000-B) exhibit a flat mode I fracture transition distance just after crack initiation. The crack propagates under plane strain state before it slants at a 45° angle. Crack propagation in these types of steel needs a minimum distance to fully develop necking, named as d_{trans}. It is shown that DENT specimens with a ratio l/d_{trans} lower than 3 give lower work of fracture and cannot be considered for the calculation of the essential work of fracture. Thus, a new criterion could be defined based on this ratio, stating that the ligament length should be at least a minimum of $3d_{trans}$ to guarantee a transition from mixed mode to quasi-plane stress state. Steels with high hardening capacity, such as DP1000-A and CFB1180, with a low necking capability exhibit a very small transition distance. Thus, small ligaments (down to 2 mm) follow the trend of *conventional* ligaments and can be used to estimate the essential work of fracture.
- Large ligaments can be used to calculate the essential work fracture if the ligaments are fully yielded prior to the onset of crack propagation. It has been verified in steels with high and low necking ability.
- The (W/3) restriction seems to have no effect on the EWF measurement and can be discarded when defining the valid ligament range.
- According to the above conclusions, the minimum and maximum ligament length to estimate the essential work of fracture are proposed. These new limits help to extend the use of the EWF methodology to different specimen geometries, with greater flexibility to characterize small specimens.

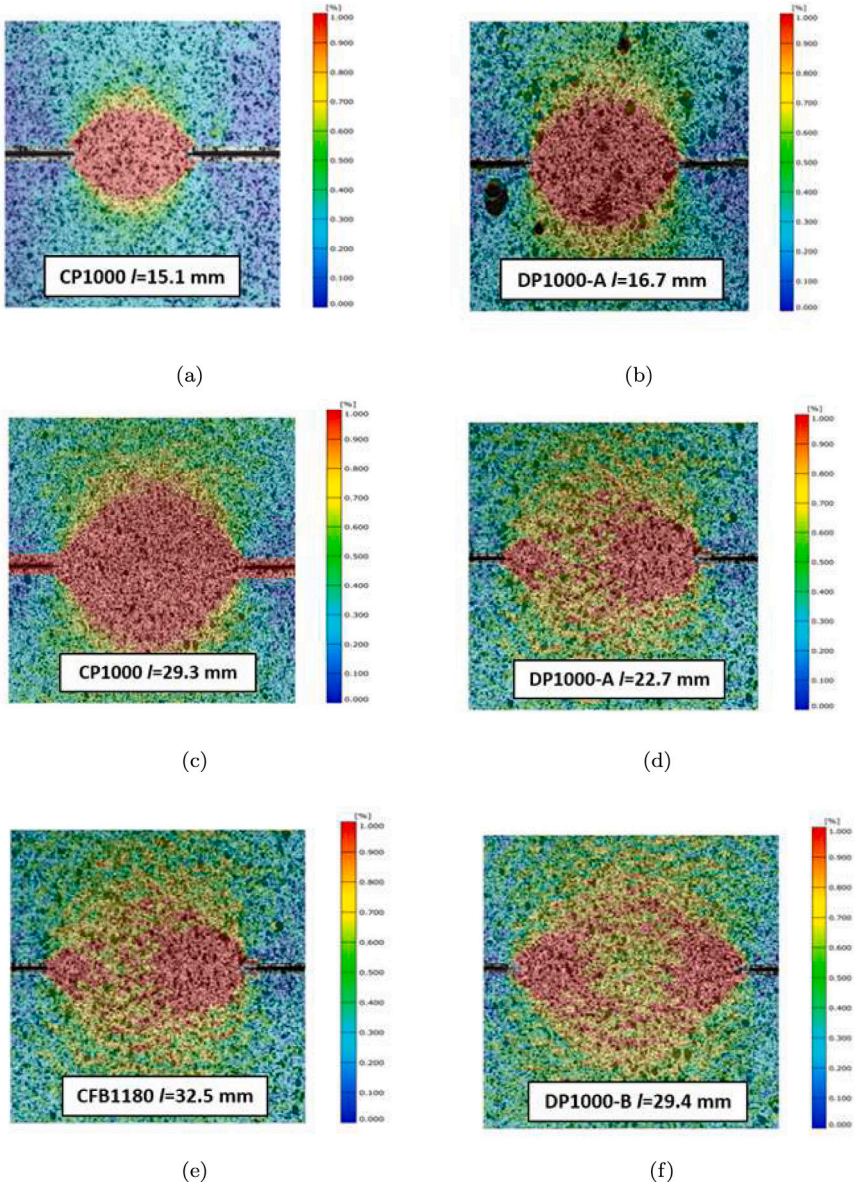

Fig. 9. DIC images at crack initiation for different ligament ranges. (a-b) Circular extension of the plastic zone in *conventional* ligaments CP1000 l = 15.1 mm and DP1000-A l = 16.7 mm; (c-f) Extension of the plastic zone in *large* ligaments range (c) CP1000 l = 29.3 mm; (d) DP1000-A l = 22.7 mm; (e) CFB1180 l = 32.5 mm; (f) DP1000-B l = 29.4 mm.

The recommended ligament lengths for high strength sheets are as follows:

- The smallest ligament size should be at least 3 times the transition distance (d_{trans}), calculated from the fracture surface of DENT specimens. In steels with low necking capacity, d_{trans} is almost negligible and ligaments as small as 2 mm can be tested.
- The maximum ligament length should be equal to Irwin's plastic zone size, estimated by means of linear elastic crack-tip stress fields.

CRediT authorship contribution statement

I. Tarhouni: Writing – original draft, Investigation. **D. Frómeta:** Writing – review & editing, Methodology, Investigation. **D. Casellas:** Writing – review & editing, Validation, Methodology, Conceptualization. **J. Costa:** Writing – review & editing, Validation, Methodology, Conceptualization. **P. Maimí:** Writing – review & editing, Validation, Methodology, Conceptualization.

Declaration of competing interest

The authors declare that they have no known competing financial interests or personal relationships that could have appeared to influence the work reported in this paper.

Acknowledgements

I.T. is a fellow of Eurecat's "Vicente López" PhD grant program. This work was partially funded by the Catalan Government through the funding grant ACCIÓ-Eurecat (project OptiLightMat). The research leading to these results has received funding from the European Union's Research Fund for Coal and Steel program under grant agreement No. 101034036 – ToughSteel project. Open Access funding provided thanks to the CRUE-CSIC agreement with Elsevier.

References

[1] Schmitt J-H, Iung T. New developments of advanced high-strength steels for automotive applications. Comptes Rendus Phys 2018;19(8):641–56.
[2] Teng Z, Chen X. Edge cracking mechanism in two dual-phase advanced high strength steels. Mater Sci Eng A 2014;618:645–53.
[3] Martin G, Veron M, Brechet Y, Chehab B, Fourmentin R, Mithieux J-D, Yerra SK, Delannay L, Pardoen T. Characterization of the hot cracking resistance using the essential work of fracture (EWF): application to duplex stainless steels. Rem: Revista Escola de Minas 2013;66:145–51.
[4] Casellas D, Lara A, Frómeta D, Gutiérrez D, Molas S, Pérez L, Rehrl J, Suppan C. Fracture toughness to understand stretch-flangeability and edge cracking resistance in AHSS. Metall Mater Trans A 2017;48(1):86–94.
[5] Frómeta D, Tedesco M, Calvo J, Lara A, Molas S, Casellas D. Assessing edge cracking resistance in AHSS automotive parts by the essential work of fracture methodology. In: J Phys: Conf Ser. 896, (1):IOP Publishing; 2017, 012102.
[6] Frómeta D, Lara A, Parareda S, Casellas D. Evaluation of edge formability in high strength sheets through a fracture mechanics approach. In: AIP conference proceedings, vol. 2113, no. 1. AIP Publishing LLC; 2019, 160007.
[7] Frómeta D, Lara A, Grifé L, Dieudonné T, Dietsch P, Rehrl J, Suppan C, Casellas D, Calvo J. Fracture resistance of advanced high-strength steel sheets for automotive applications. Metall Mater Trans A 2021;52(2):840–56.
[8] Frómeta D, Lara A, Molas S, Casellas D, Rehrl J, Suppan C, Larour P, Calvo J. On the correlation between fracture toughness and crash resistance of advanced high strength steels. Eng Fract Mech 2019;205:319–32.
[9] Standard A, et al. Standard test method for linear-elastic plane-strain fracture toughness KIc of metallic materials. 2012, ASTM Book of Standards, ASTM International West Conshohocken, PA.
[10] Standard A, et al. Standard test method for measurement of fracture toughness. 2001, p. 1–46, ASTM, E1820-01.
[11] Frómeta D, Parareda S, Lara A, Molas S, Casellas D, Jonsén P, Calvo J. Identification of fracture toughness parameters to understand the fracture resistance of advanced high strength sheet steels. Eng Fract Mech 2020;229:106949.
[12] Mai Y, Pilko K. The essential work of plane stress ductile fracture of a strain-aged steel. J Mater Sci 1979;14(2):386–94.
[13] Marchal Y, Delannay F. Comparison of methods for fracture toughness testing of thin low carbon steel plates. Mater Sci Technol 1998;14(11):1163–8.
[14] Mai Y, Cotterell B. The essential work of fracture for tearing of ductile metals. Int J Fract 1984;24(3):229–36.
[15] Pardoen T, Hachez F, Marchioni B, Blyth P, Atkins A. Mode I fracture of sheet metal. J Mech Phys Solids 2004;52(2):423–52.
[16] Cotterell B, Reddel J. The essential work of plane stress ductile fracture. Int J Fract 1977;13(3):267–77.
[17] Cotterell B, Pardoen T, Atkins A. Measuring toughness and the cohesive stress–displacement relationship by the essential work of fracture concept. Eng Fract Mech 2005;72(6):827–48.
[18] Pardoen T, Marchal Y, Delannay F. Essential work of fracture compared to fracture mechanics—Towards a thickness independent plane stress toughness. Eng Fract Mech 2002;69(5):617–31.
[19] Lacroix G, Pardoen T, Jacques PJ. The fracture toughness of TRIP-assisted multiphase steels. Acta Mater 2008;56(15):3900–13.
[20] Gutiérrez D, Pérez L, Lara A, Casellas D, Prado J. Toughness evaluation of high strength steels sheets by means of the essential work of fracture. In: 19t H European conference on fracture: fracture mechanics for durability, reliabilit Y and safety. Citeseer; 2012.
[21] MR SK, Schmidova E, Konopík P, Melzer D, Bozkurt F, V Londe N. Fracture toughness analysis of automotive-grade dual-phase steel using essential work of fracture (EWF) method. Metals 2020;10(8):1019.
[22] Sarkar R, Chandra SK, De PS, Chakraborti P, Ray S. Evaluation of ductile tearing resistance of dual-phase DP 780 grade automotive steel sheet from essential work of fracture (EWF) tests. Theor Appl Fract Mech 2019;103:102278.
[23] Pujante J, Frómeta D, Garcia-Llamas E, Gimenez M, Casellas D. Hot stamped aluminium for crash-resistant automobile safety cage applications. In: Mater Sci Forum, vol. 1016. Trans Tech Publ; 2021, p. 445–52.
[24] Barany T, Czigány T, Karger-Kocsis J. Application of the essential work of fracture (EWF) concept for polymers, related blends and composites: A review. Prog Polym Sci 2010;35(10):1257–87.
[25] Clutton E. Essential work of fracture. In: European structural integrity society, vol. 28. Elsevier; 2001, p. 177–95.
[26] Pardoen T, Marchal Y, Delannay F. Thickness dependence of cracking resistance in thin aluminium plates. J Mech Phys Solids 1999;47(10):2093–123.
[27] Tuba F, Oláh L, Nagy P. The role of ultimate elongation in the determination of valid ligament range of essential work of fracture tests. J Mater Sci 2012;47(5):2228–33.
[28] Tuba F, Oláh L, Nagy P. On the valid ligament range of specimens for the essential work of fracture method: The inconsequence of stress criteria. Eng Fract Mech 2013;99:349–55.
[29] Marchal Y, Walhin J-F, Delannay F. Statistical procedure for improving the precision of the measurement of the essential work of fracture of thin sheets. Int J Fract 1997;87(2):189–99.
[30] Marchal Y, Delannay F. Influence of test parameters on the measurement of the essential work of fracture of zinc sheets. Int J Fract 1996;80(4):295–310.
[31] Martinez A, Gamez-Perez J, Sanchez-Soto M, Velasco JI, Santana O, Maspoch ML. The essential work of fracture (EWF) method–analyzing the post-yielding fracture mechanics of polymers. Eng Fail Anal 2009;16(8):2604–17.
[32] Frómeta D, Parareda S, Lara A, Grifé L, Tarhouni I, Casellas D. A new cracking resistance index based on fracture mechanics for high strength sheet metal ranking. IOP Conf Ser: Mater Sci Eng 2021;1157(1):012094.
[33] Wu J, Mai Y-W, Cotterell B. Fracture toughness and fracture mechanisms of PBT/PC/im blend. J Mater Sci 1993;28(12):3373–84.
[34] Arkhireyeva A, Hashemi S. Fracture behaviour of polyethylene naphthalate (PEN). Polymer 2002;43(2):289–300.
[35] Arkhireyeva A, Hashemi S. Combined effect of temperature and thickness on work of fracture parameters of unplasticized PVC film. Polym Eng Sci 2002;42(3):504–18.
[36] Hashemi S. Temperature dependence of work of fracture parameters in polybutylene terephthalate (PBT). Polym Eng Sci 2000;40(6):1435–46.
[37] ISO E. 6892-1. Metallic Materials-tensile testing-Part 1: Method of test at room temperature. 2009, International Organization for Standardization.

[38] Cai M-h, Ding H, Tang Z-y, Lee H-y, Lee Y-k. Strain hardening behavior of high performance FBDP, TRIP and twip steels. Steel Res Int 2011;82(3):242–8.
[39] Frómeta D, Cuadrado N, Rehrl J, Suppan C, Dieudonné T, Dietsch P, Calvo J, Casellas D. Microstructural effects on fracture toughness of ultra-high strength dual phase sheet steels. Mater Sci Eng A 2021;802:140631.
[40] Saleemi A, Nairn J. The plane-strain essential work of fracture as a measure of the fracture toughness of ductile polymers. Polym Eng Sci 1990;30(4):211–8.
[41] Sarkara R, Chandraa S, De P, Chakraborti P, Ray S. Evaluation of ductil e tearing resistance of dual-phase DP 780 grade automotive steel sheet from essentia l work of fracture (EWF) tests. Theor Appl Fract Mec 2019;103:102278.
[42] Anderson TL. Fracture mechanics: fundamentals and applications. CRC Press; 2017.
[43] Morgeneyer TF, Besson J. Flat to slant ductile fracture transition: Tomography examination and simulations using shear-controlled void nucleation. Scr Mater 2011;65(11):1002–5.
[44] Knockaert R, Doghri I, Marchal Y, Pardoen T, Delannay F. Experimental and numerical investigation of fracture in double-edge notched steel plates. Int J Fract 1996;81(4):383–99.
[45] Tracey DM. Strain-hardening and interaction effects on the growth of voids in ductile fracture. Eng Fract Mech 1971;3(3):301–15.
[46] Buljac A, Hild F, Helfen L, Morgeneyer TF. On deformation and damage micromechanisms in strong work hardening 2198 T3 aluminium alloy. Acta Mater 2018;149:29–45.
[47] Tekoğlu C, Hutchinson J, Pardoen T. On localization and void coalescence as a precursor to ductile fracture. Phil Trans R Soc A 2015;373(2038):20140121.
[48] Luo Z, Huang M. Revealing the fracture mechanism of twinning-induced plasticity steels. Steel Res Int 2018;89(9):1700433.
[49] Khan I, Bhasin V. On the role of secondary voids and their distribution in the mechanism of void growth and coalescence in porous plastic solids. Int J Solids Struct 2017;108:203–15.
[50] GOM. ARAMIS user manual Reva – Software. 2009, GOM, Braunschweig, Germany, 2009, GOM, Braunschweig, Germany.